Gecko

Design for IGA-type discretization workflows

Gecko Technical Report 2

DC10 – Wei LI

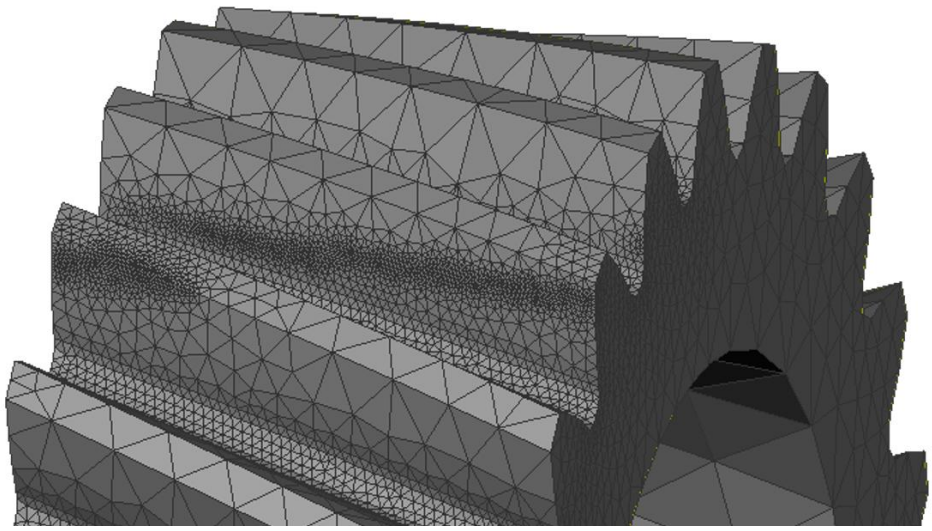

This project has received funding from the European Union's Horizon Europe research and innovation program under grant agreement No 101073106
Call: HORIZON-MSCA-2021-DN-01

Funded by the European Union

Executive summary

This report presents the advancements achieved in the GECKO project within the framework of Horizon 2020, with a focus on the development and application of IGA for contact mechanics.

Building upon the previously developed IGA framework, the present work focused on the implementation and validation of a penalty-based contact formulation for 2D and 3D applications, including Hertzian cylinder contact benchmark cases.

Subsequently, the developed framework was applied to gear contact analysis, extending from 2D gear models to 3D spur gear simulations. The numerical results showed very good agreement with analytical Hertzian solutions, demonstrating the accuracy and robustness of the proposed IGA-based contact methodology.

Table of contents

List of figures

List of tables

List of abbreviations

IGA	*Iso Geometric Analysis*

Introduction

This document presents the research progress achieved within the GECKO Project on the development and application of IGA for contact mechanics problems, with emphasis on Hertzian and gear contact analysis.

The structure of this deliverable is organized as follows. Section 1 presents the numerical validation studies, including 2D and 3D Hertzian contact benchmark cases. Section 2 introduces the application of the developed framework to 2D and 3D spur gear contact analysis. Finally, the main conclusions and future outlook are summarized in Section 3.

As discussed by Lu [1], the two-pass algorithm improves the stability and accuracy of contact pressure computations by performing independent contact evaluations on each surface and averaging the resulting stiffness matrices and residuals. This approach effectively eliminates geometric bias and ensures more reliable contact stress distributions. Based on the accuracy investigations reported in [2] and [3], cubic IGA basis functions were adopted for the description of the gear involute geometry, while quadratic basis functions were employed in the remaining directions. The analytical solution is calculated according to Hertzian theory and ISO 6336-2 [4].

Both 2D and 3D concentrated contact and gear contact models ($E = 208 \times 10^3$ N/mm^2, $\nu = 0.28$) are simulated and validated against analytical Hertzian solution. The 2D contact problem is formulated under the plane strain assumption.

1 Concentrated Contact Validation

1.1. 2D Hertzian Contact

In the 2D configuration (Fig. 1a), contact between two cylinders with diameters of 10 mm and 20 mm respectively, is analyzed in the xy-plane. A compressive normal load of 100 N is applied to establish contact. Rigid body motion is prevented by constraining the displacement in the x-direction along the left boundary.

Fig. 1b illustrates the globally refined mesh used in the analysis, whereas Fig. 1c shows the locally refined mesh concentrated in the anticipated contact region. The minimum element size in the x-direction within the refined zone is approximately 0.01 mm and 0.03 mm, respectively.

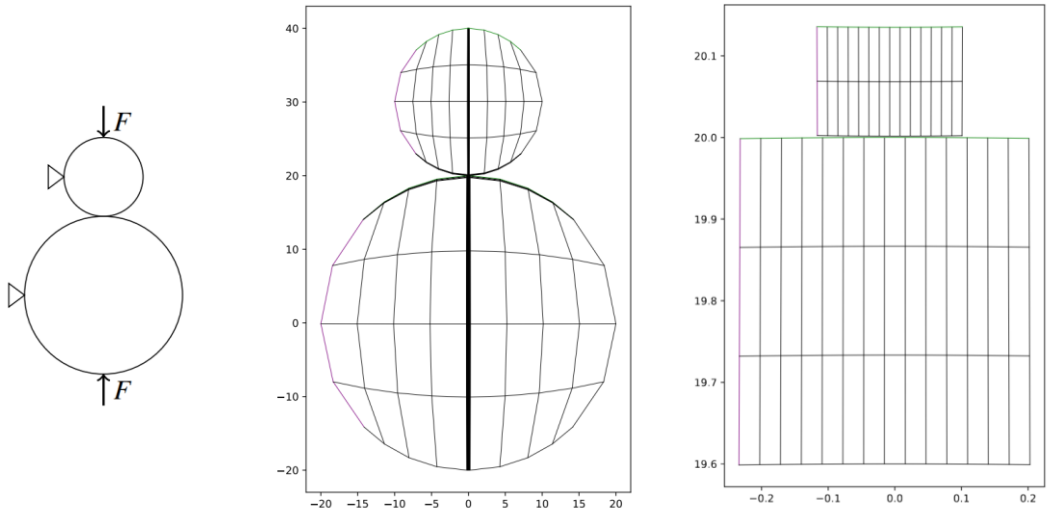

(a) 2D cylinder contact model.

(b) Global mesh.

(c) Local mesh refinement.

Figure 1: Geometry and mesh discretization of the 2D Hertzian cylinder contact problem.

The penalty parameter ε_n is set as $120 * E$. The resulting contact pressure distribution agrees closely with the analytical Hertzian solution (Fig. 2(b)).

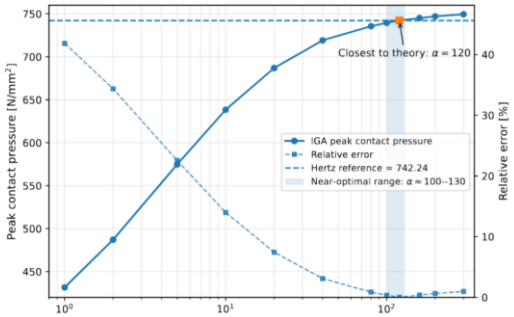

(a) Penalty parameter sensitivity.

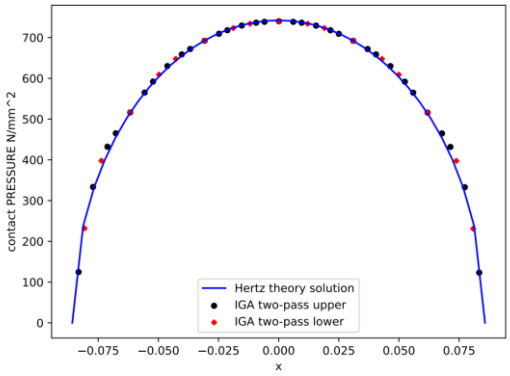

(b) Contact pressure distribution.

Figure 2: Contact response of the 2D Hertzian cylinder problem.

1.2. 3D Hertzian Cylinder Contact

The 3D cylinder model is generated by extruding the 2D geometry in Fig. 1a along the z-axis to a length of 10 mm. A uniform compressive line load 10 N/mm is applied. Rigid body motion is suppressed by constraining the left boundary in the x- and z- directions. The 3D cylinder is discretized with 16 elements along the axial (z) direction, resulting in an average mesh size of 0.625 mm, to accurately resolve the contact behavior across the finite width.

Fig. 3a and Fig. 3b illustrate the distributions of the maximum contact pressure and the normal contact force along the width direction, respectively. The contact pressure and the contact force remain nearly constant in the inner region and decreases toward the boundaries, indicating the presence of finite-length effects.

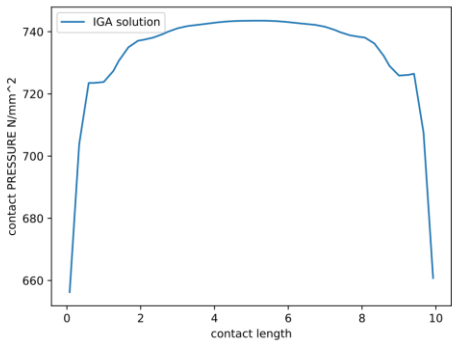

(a) Contact pressure distribution along the face width.

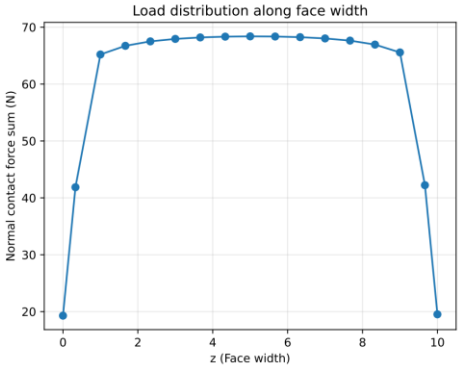

(b) Contact force distribution along the face width.

Figure 3: Contact response of the 3D Hertzian cylinder problem along the face-width direction.

Fig. 4a presents the contact pressure profile along the contact coordinate *x* at the mid-plane *z* = *L*/2. Since the mid-plane is least affected by finite-length effects, the numerical results closely follow the analytical Hertzian solution, indicating an accurate resolution of the local contact behavior. Fig. 4b shows the contact pressure evaluated at all Gauss integration points on the cylindrical contact surface. The numerical points form a family of Hertz-like pressure profiles, with small variations in the peak pressure along the width direction due to finite-length effects. The maximum pressure fluctuates slightly around the theoretical Hertzian value, which is consistent with the trend observed in Fig. 3a.

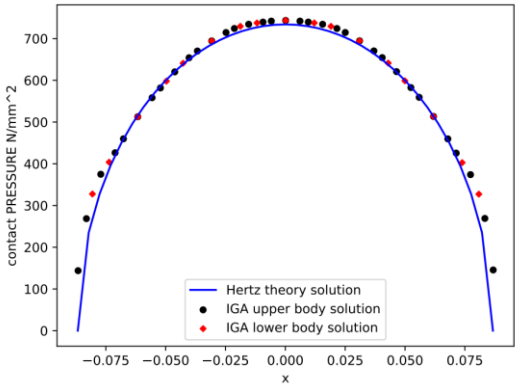

(a) Contact pressure distribution at the mid-plane

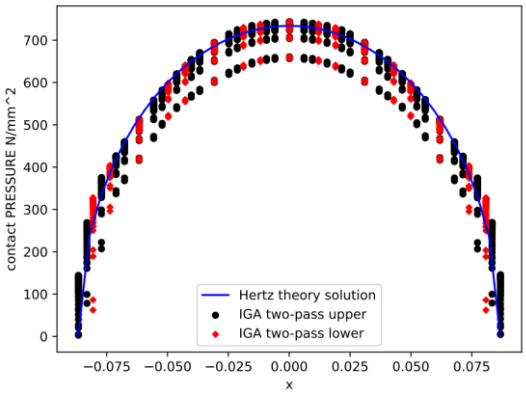

(b) Contact pressure distribution at all in-contact Gauss integration points.

Figure 4: Contact pressure distribution on 3D cylinder.

2 2D Gear Contact Analysis

A 2D spur gear pair with exact involute profiles is considered for the contact analysis on the transverse plane (*x*–*y* plane). The key operating parameters at the contact position are summarized in Table 1. Here, d_w is the working pitch diameter. ρ denote the radii of curvature at the contact point which will be used in the Hertzian approximation. F_n is the normal contact force along the line of action. For the ideal 2D Hertzian contact, the maximum contact pressure σ_{H0} and the half-width of the contact zone $b_0/2$ can be derived analytically and they are used as reference solutions. The Hertzian reference values reported in Table 1 are computed assuming a face width of 10 mm. In contrast, the 2D gear contact model is formulated under plane strain conditions with a unit thickness of 1 mm. Therefore, to ensure consistency with the Hertzian solution, the applied torque in the simulation is scaled down by a factor of 10. The following material elastic properties are set E = 208×10^3 N/mm^2, ν = 0.28.

Fig. 5a illustrates the NURBS discretization of the 2D gear pair. The pinion and gear are positioned in the lower right and upper-left regions of the domain, respectively. Candidate contact boundaries are explicitly defined on both bodies, and a driving torque is applied along the lower boundary of the pinion. Displacement constraints are imposed on the gear body to eliminate rigid body motion, the bottom boundary is fixed in both *x*- and *y*-directions. Strong local refinement is introduced near the potential contact interface to capture high pressure gradients, with a minimum element size of h_{min} = 0.0057 mm.

Table 1: Geometric and Contact Parameters at the Contact Point of the 2D Gear Pair

Symbol	Pinion	Gear
d_w	14.75 mm	27.24 mm
α_{wt}	29.05°	
ρ	3.58 mm	6.61 mm
T	375 $N \cdot mm$	
Fn	58.14 N	
σ_{H0}	299.852 N/mm^2	
$b0/2$	0.012 mm	

To represent the contact pressure distribution along the interface, a curvilinear abscissa is constructed from the spatial coordinates of the contact Gauss points. The incremental arc length on the pinion side is defined as

$$\Delta s_i = ||x_{i+1} - x_i|| \tag{1}$$

where $X_i$denotes the *i*-th Gauss point. The cumulative coordinate is given by

$$s_i = \sum_{k=1}^{i} \Delta s_k \tag{2}$$

For symmetry in visualization, the abscissa is centered as

$$s_i^c = s_i - (s_{min} + s_{max})/2 \tag{3}$$

where s_i^cdenotes the centered coordinate.

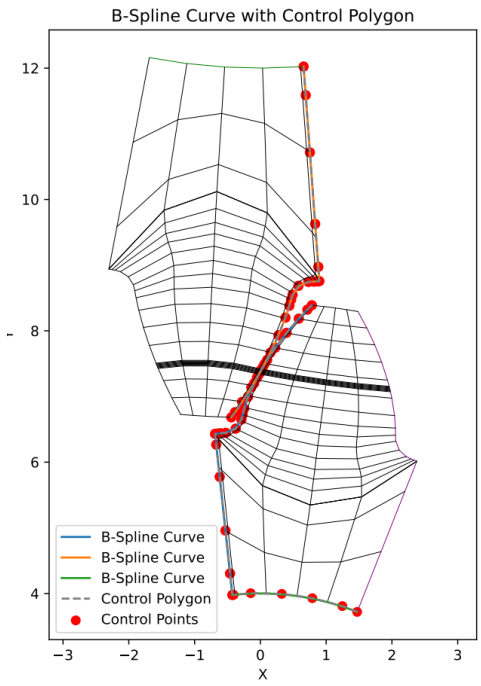

(a) NURBS mesh and local refinement near the contact interface.

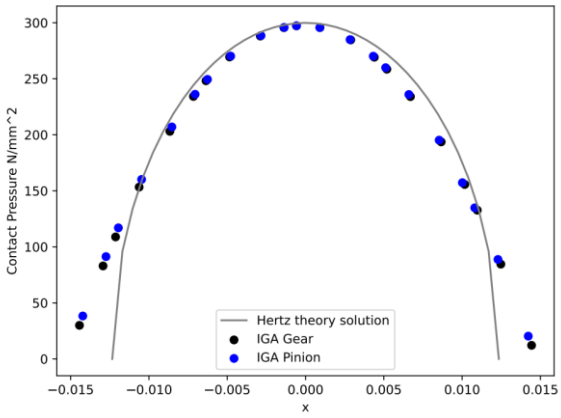

(b) Contact pressure distribution of the 2D gear pair.

Figure 5: 2D gear contact model and its contact pressure distribution.

The contact pressure distribution as a function of the centered abscissa s^c is shown in Fig. 5b. The solution exhibits the characteristic Hertzian profile, with a symmetric distribution and a maximum at the center of the contact region. The maximum contact pressure is 297.28 N/mm2, and the contact half-width is 0.015 mm.

Fig. 6 presents the stress distribution of the 2D gear pair, including both the global and local views. In the global stress field (Fig. 6a), the stress is predominantly low over most of the domain, with a clear concentration emerging at the contact region. This indicates that the load transfer is highly localized, as expected in gear contact problems. The local stress field (Fig. 6b) provides a detailed view of the contact zone, where a pronounced stress concentration is observed at the contact interface. The stress distribution exhibits a smooth gradient away from the contact region, reflecting the continuous nature of the NURBS-based discretization.

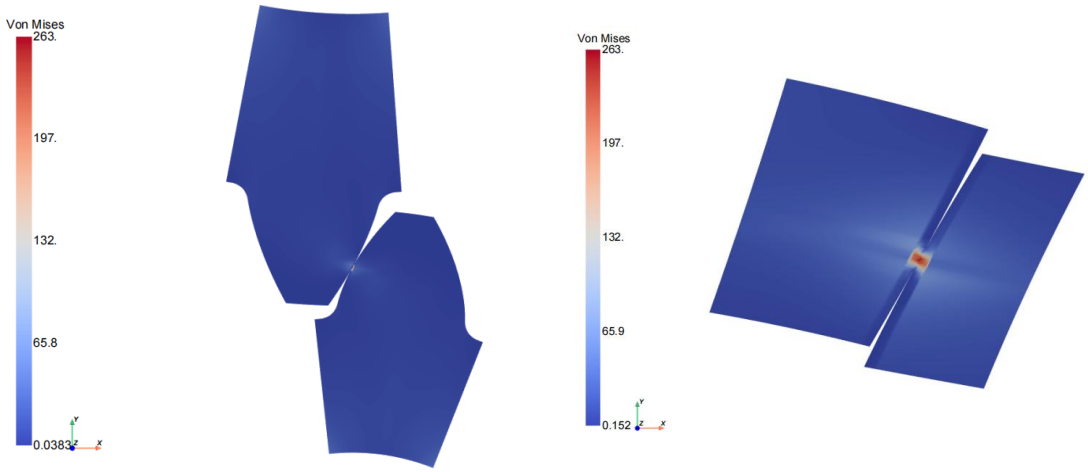

(a) Global stress field. (b) Local stress field.

Figure 6: 2D gear stress distribution.

Fig. 7 illustrates the strong dependence of the penalty-based IGA contact formulation on the penalty parameter. Increasing the penalty factor reduces the normal penetration, indicating a stiffer contact interface. Nevertheless, excessively large penalty values lead to artificial over-stiffening and an unrealistic increase in the computed contact pressure. Hence, an appropriate penalty parameter should balance penetration control and contact-pressure accuracy. An intermediate range of α in [20, 40] is therefore recommended in this case, providing a good balance between accuracy and numerical stability. Accordingly, α = 30 is adopted in the present 2D study.

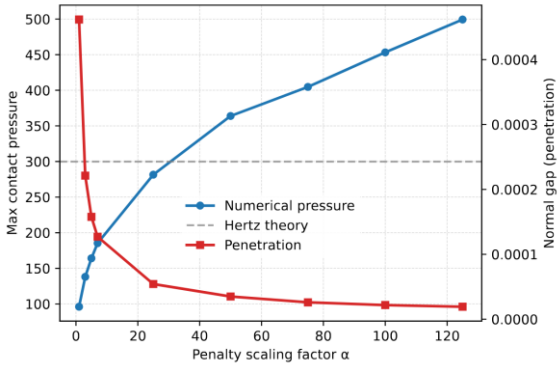

Figure 7: Effect of the penalty scaling factor on the contact response.

3 3D Spur Gear Contact Analysis

The validated 2D involute tooth profiles were extruded along the axial (z) direction to generate the corresponding three-dimensional spur gear pair. This extrusion procedure preserves the exact involute geometry in the transverse plane while introducing a finite face width, thereby enabling the investigation of load distribution and contact stress variation along the tooth width. Both the pinion and the gear were discretized using NURBS-based Isogeometric solid elements, ensuring geometric exactness and high-order continuity across the contact interface. The penalty factor is chosen as $50 * E$ for the single-pair tooth contact. However, the two-pass integration method fails to achieve convergence in the 3D spur gear contact analysis. Therefore, the one-pass method is adopted.

The driving torque is transformed into circumferential force, and applied to pinion. Two representative torque transmission scenarios were considered, Fig. 8a. In the first case, the input driving torque was assumed to be uniformly distributed along the face width. The loading condition represents the ideal Power transmission. In the second case, a non-uniform loading condition was prescribed in which the transmitted torque decreases linearly along the face width direction. This assumption is motivated by practical transmission systems, where the driving power is typically introduced at one end of the gear shaft. As a result, the load transfer along the shaft is not uniform, and a progressive reduction of torque occurs toward the free end of the face width. The resulting normal contact force distributions along the face width are shown in Fig. 8b. For the uniform case, the contact force remains nearly constant, indicating homogeneous load transfer. In contrast, the linear torque case produces a proportional variation in contact force, directly following the imposed load gradient.

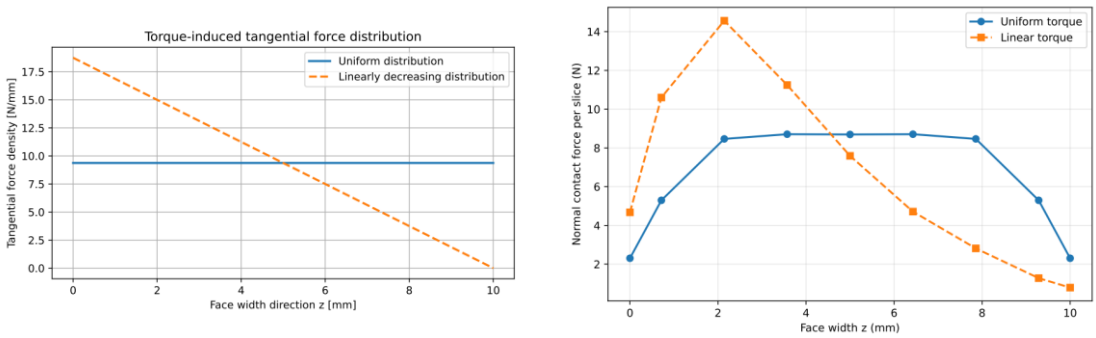

(a) Torque distribution.

(b) Contact force distribution along face width.

Figure 8: Torque and contact force on 3D spur gear.

Under uniform torque, both the stress field (Fig. 9a) and contact pressure (Fig. 10a) exhibit a nearly uniform distribution along the face width, indicating balanced load sharing. Under the linearly decreasing torque, a pronounced axial gradient is observed. The stress (Fig. 9b) and contact pressure (Fig. 10b) both decrease progressively away from the driving side, consistent with the prescribed load distribution. These results demonstrate that the proposed framework accurately captures load redistribution effects induced by non-uniform torque transmission.

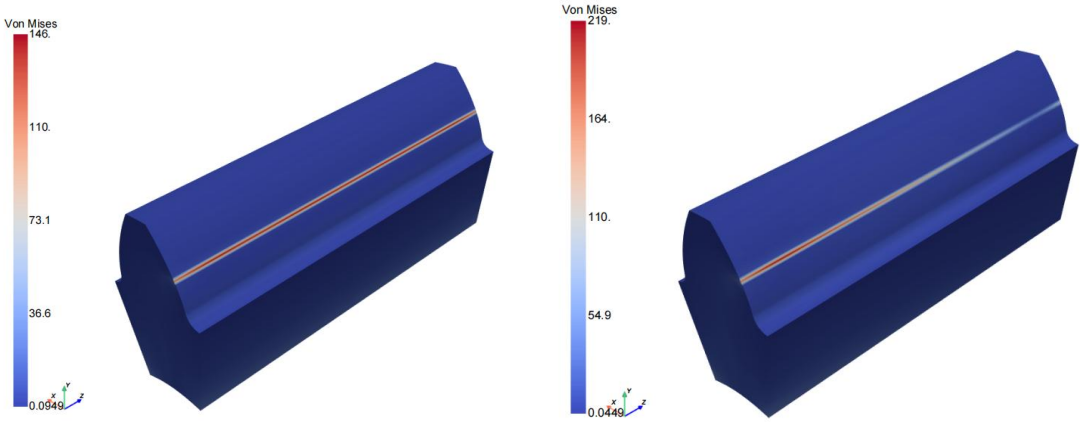

(a) Uniform stress distribution.

(b) Un-uniform stress distribution along face width.

Figure 9: Stress distribution of pinion along the face width.

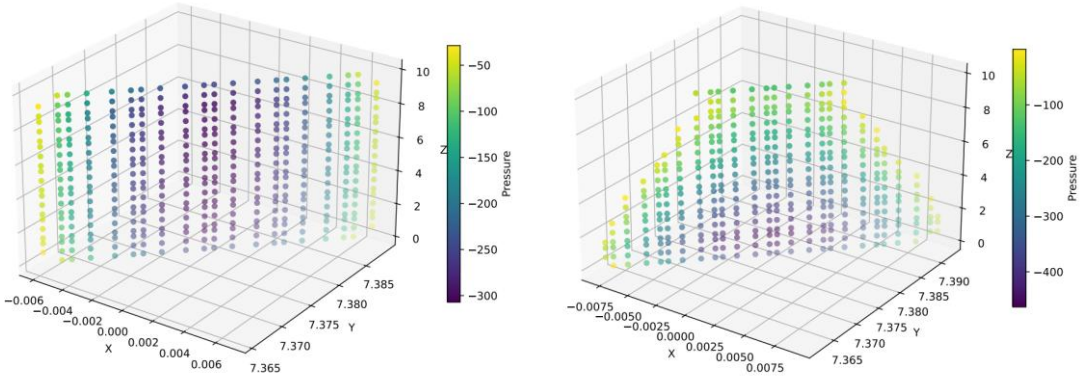

(a) Contact pressure distribution under uniform driving force.

(b) Contact pressure distribution under un-uniform driving force.

Figure 10: Contact pressure distribution of pinion along the face width.

4 CONCLUSIONS

This report presented the development and validation of a penalty-based IGA framework for contact mechanics applications, with emphasis on gear contact analysis. The methodology was systematically verified through 2D and 3D Hertzian contact benchmark problems and subsequently extended to spur gear contact simulations.

The obtained numerical results showed very good agreement with analytical Hertzian solutions and theoretical predictions, confirming the accuracy and robustness of the proposed contact formulation. In addition, the developed framework successfully captured stress distributions, contact pressure variations, and load redistribution effects under different torque transmission conditions.

The presented work establishes a solid foundation for future extensions toward more advanced gear contact problems, particularly the analysis of helical gear systems and more realistic 3D contact conditions.

5 REFERENCES

[1] Jia Lu. *Isogeometric contact analysis: Geometric basis and formulation for frictionless contact.* Computer Methods in Applied Mechanics and Engineering, 200(5–8):726–741, 2011.

[2] Andreas Beinstingel, Michael Keller, Michael Heider, Burkhard Pinnekamp, and Steffen Marburg. *A hybrid analytical-numerical method based on isogeometric analysis for determination*

[3] Christos Karampatzakis, Angelos Mantzaflaris, Christopher Provatidis, and Athanassios Mihailidis. *Adaptive isogeometric gear contact analysis: Geometry generation, truncated hierarchical B-spline refinement and validation.* Computers & Structures, 305:107553, 2024.

[4] Calculation of load capacity of spur and helical gears — part 2: Calculation of surface durability (pitting), 2019. Third edition, corrected version 2020.